Chalcogenide Letters Vol. 11, No. 10, October 2014, p. 485 - 491

EFFECT OF VACUUM ANNEALING ON THE PROPERTIES OF SPUTTERED SnS THIN FILMS

J. XU*, Y. YANG, Z. XIE
School of Materials and Energy, Guangdong University of Technology, Guangzhou 510006, China

The semiconducting SnS thin films were deposited by magnetron sputtering with a SnS composite target. The effects of vacuum annealing on the structural, compositional, morphological, and optical properties of sputtered SnS thin films were studied. The experimental results show that the X-ray diffraction peaks of SnS and grain sizes enhance significantly with increasing annealing temperature. The compositions of prepared thin films are close to the stoichiometry of SnS. The increased annealing temperature leads to the enlargements of cracks and voids in the surface of thin films. The optical band gaps of SnS thin films change slightly with the annealing temperature.

(Received August 21, 2014; Accepted October 3, 2014)

Keywords: SnS; Annealing; Thin films; Sputtering; Structural

1. Introduction

In recent years, the thin film solar cells have received much attention due to their advantages of reduced thickness and low cost. Among the thin film solar cells, the $Cu(In,Ga)Se_2$ thin film solar cells have reached the maximum conversion efficiency of 20.8% [1]. However, the abundance of indium element in the earth's crust is less than 0.05 ppm [2]. Besides, the $Cu(In,Ga)Se_2$ thin film solar cells usually contain toxic cadmium element because CdS thin films are typically used as buffer layer. Therefore, it's necessary to develop environment-friendly materials as solar cell absorbers. The binary sulfide SnS thin films have been considered to be promising alternates [3–8]. The Sn and S elements are nontoxic and abundant in the earth's crust (Sn: 2.2 ppm and S: 260 ppm) [2]. The SnS thin films usually show p-type conductivity. The optical absorption coefficients of SnS thin films are 10^4-10^5 cm^{-1} [9,10]. The reported band gaps of SnS thin films are 1.3-1.5 eV, which fit the optimal band gap value for single junction solar cells [6,10–14].

The SnS thin films can be prepared by evaporation [3,4,11], PECVD [5], sulfurization [6,12,13], spray pyrolysis [7], sol-gel [8], chemical bath deposition [14], and electrochemical deposition [15,16], etc. In addition to the above methods, the magnetron sputtering shows advantages of low temperature rise during deposition, high deposition rate, good adhesion between the thin film and substrate, and good uniformity of thin films, etc. However, there are little reports about the fabrication of SnS thin films by magnetron sputtering [9,10,17]. Besides, the post heat treatment in the vacuum has not been applied to the sputtered SnS thin films in the literature.

In this study, we tried to enhance the properties of sputtered SnS thin films by vacuum annealing. The SnS thin films were deposited on soda-lime glass substrates by magnetron sputtering and post vacuum annealing. The influences of annealing temperature on the structural, compositional, morphological, and optical properties of thin films were investigated.

*Corresponding author xujiaxiong@gdut.edu.cn

2. Experimental methods

The SnS thin films were sputtered and annealed by a FJL560 magnetron sputtering system. The soda-lime glasses were used as substrates. Using ultrasonic cleaning, the substrates were successively rinsed in the acetone, alcohol, and deionized water. Then, they were transferred to the magnetron sputtering chamber. A SnS target with the purity of 99.999% and Sn:S=1:1 in atomic ratio was used. The magnetron sputtering chamber was pumped to 4×10^{-4} Pa. Then, the pure argon with a flow of 20 ml/min was introduced into the chamber as sputtering gas and the chamber pressure was kept at 0.5 Pa. The radio frequency (RF) sputtering with a frequency of 13.56 MHz was utilized for thin film depositions. The forward power, reflective power, and self-bias were 100 W, 1 W, and 120 V, respectively. All depositions were made keeping the substrates at room temperature. The deposited time was 45 min. The as-deposited thin films were in-situ annealed in the sputtering chamber without breaking the vacuum condition. Compared with the traditional annealing method, the in-situ annealing can avoid the possible pollutions during the transfer of samples from the sputtering chamber to the annealing furnace. It can also save total time of fabrication. The chamber pressure was less than 9×10^{-4} Pa during annealing. The annealing temperatures were 300 °C, 400 °C, and 500 °C. The annealing time was 1 hour.

The structural properties of SnS thin films were identified by X-ray diffractometry (XRD, Rigaku D/MAX-Ultima IV). The surface morphologies and compositions of SnS thin films were characterized by scanning electron microscopy (SEM, Hitachi S3400N) with an energy dispersive spectroscopy (EDS) detector. The optical properties of SnS thin films were measured by UV–Vis spectrophotometry (Shimadzu, UV-2450).

3. Results and discussion

Fig. 1 shows the XRD patterns of as-deposited and annealed thin films. The XRD pattern of as-deposited thin films shows only a weak diffraction peak from the (040) plane of SnS, which reveals the formation of crystalline SnS structure before annealing. K. Hartman et al. have reported that polycrystalline SnS thin films can be prepared by sputtering at room temperature [9]. However, in this study, the crystallinity of SnS thin films prepared at room temperature is still weak. Thus, we performed a vacuum annealing, in order to improve the crystallinity of SnS thin films. As seen in Fig. 1, a significant (040) peak is observed for thin films annealed at 300 °C. The peak intensity is about 3 times to that of as-deposited thin films. Besides, the peaks attributed to the (120), (131), and (151) planes of SnS appear in the XRD pattern. Thus, the crystallinity of SnS thin films improves evidently after vacuum annealing. When the annealing temperatures increase to 400 °C and 500 °C, the intensity of (040) peaks enhances continuously. The XRD pattern of thin films annealed at 500 °C contains peaks corresponding to the (120), (021), (101), (040), (131), (151), and (042) planes of SnS. The preferred orientation in the (040) plane is consistent with other report [8]. As reported in the literature, the other binary sulfides (such as SnS_2 and Sn_2S_3) easily form in the fabricated SnS thin films [9,12,13]. But in Fig. 1, the peaks from other sulfides have not been detected in all the XRD patterns. Therefore, the thin films fabricated in this study are single phase of SnS. In Ref. [9], a non-stoichiometric SnS target with the composition of Sn:S≈4:6 in atomic ratio was used for sputtering, which may be the reason of the formation of other sulfides. In Refs. 12 and 13, the thin films were prepared by the sulfurization of Sn thin films. According to the Sn-S phase diagram, there are different stoichiometric compounds in the Sn-S system. Therefore, different sulfides can be formed depending on the sulfurization conditions. In this study, the SnS target was stoichiometric and it can avoid the formation of other sulfides.

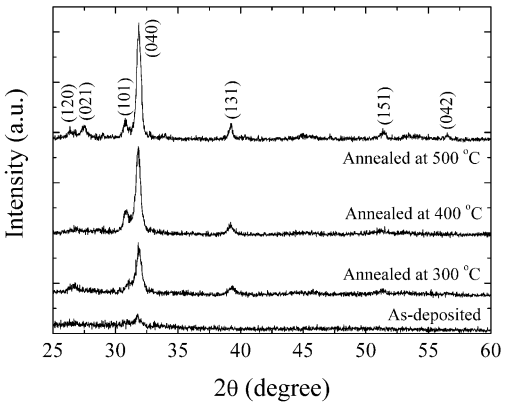

Fig. 1 The XRD patterns of as-deposited and annealed SnS thin films.

Table 1 lists the intensity, full width at half maximum (FWHM), and position of the (040) peak and the corresponding D-spacing and grain size against the annealing temperature. The results for the as-deposited SnS thin films are also presented in Table 1. As shown in Table 1, the peak intensities enhance and the FWHM values reduce monotonously with increasing annealing temperature. According to the Debye-Scherrer equation, the grain sizes of SnS thin films increase with the annealing temperature. The maximum grain size is 23.3 nm when the annealing temperature is 500 °C. The peak positions are almost unchanged with the annealing temperature. So the change in the D-spacing can be neglected.

Table 1 The intensity, FWHM, and position of the (040) peak and the corresponding D-spacing and grain size with the annealing temperature.

Annealing temperature	Intensity (a.u.)	FWHM (°)	Position (°)	D-spacing (nm)	Grain size (nm)
As-deposited	387	0.599	31.83	2.809	13.6
300 °C	1107	0.447	31.82	2.810	18.3
400 °C	1820	0.442	31.82	2.810	18.5
500 °C	2380	0.350	31.86	2.807	23.3

Fig. 1 and Table 1 reveal that vacuum annealing can enhance the crystallinity of SnS thin films. The energies provided by annealing can promote the crystal growth of deposited thin film, leading to enhanced XRD peaks and enlarged grain sizes with increasing annealing temperature. Due to the limit of thermal stability of glass substrates, we did not further increase the annealing temperature of thin films.

Fig. 2 shows the EDS patterns and Table 2 lists the atomic ratios of Sn and S elements of the fabricated thin films. As seen in Table 2, the atomic ratios of Sn and S of all thin films are close to 1:1. Besides, no other elements were detected in the EDS measurements, except those from the glass substrates. Therefore, the as-deposited and annealed thin films are SnS structures, which are consistent with the XRD results. A slight reduction in the sulfur ratio with increasing annealing temperature is observed in Table 2. The reduced sulfur ratio was also reported for the evaporated SnS thin films by annealing [3,18]. Due to the volatility of sulfur, it happens some evaporation of

sulfur at higher annealing temperatures. Therefore, the Sn/S values of thin films reduce with the increase of annealing temperature.

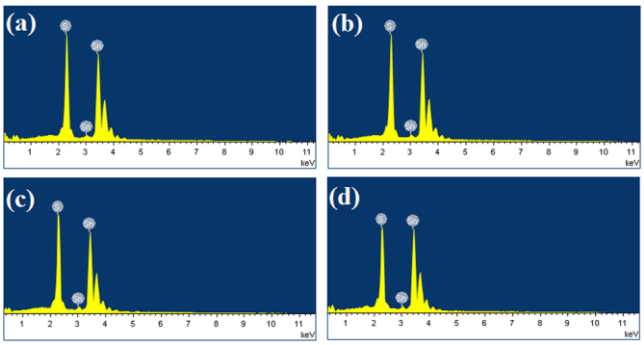

Fig. 2 The EDS patterns of (a) as-deposited thin films and thin films annealed at (b) 300 ℃, (c) 400 ℃, and (d) 500 ℃.

Table 2 The measured compositions of SnS thin films.

Annealing temperature	Sn (at.%)	S (at.%)	Sn/S
As-deposited	48.72	51.28	0.95
300 °C	49.16	50.84	0.97
400 °C	49.17	50.83	0.97
500 °C	53.76	46.24	1.16

Fig. 3 shows the SEM images of as-deposited and annealed thin films. The magnification of the SEM images is 40.0 k. The surface morphologies of all thin films are of grainy aspect. For thin films annealed at 300 °C, the surface becomes significantly compact as compared with as-deposited thin films. Besides, the agglomeration of grains, enlarged grain sizes, and micro-cracks are observed. In Fig. 3(c), the grains become irregular and the cracks are clearly observed. When the annealing temperature reaches 500 °C, the cracks and voids become more significant. It is attributed to the mismatch of thermal expansion coefficients between SnS thin films and glass substrates (2.8×10^{-7} K^{-1} and 85×10^{-7} K^{-1} for the SnS and glass respectively).

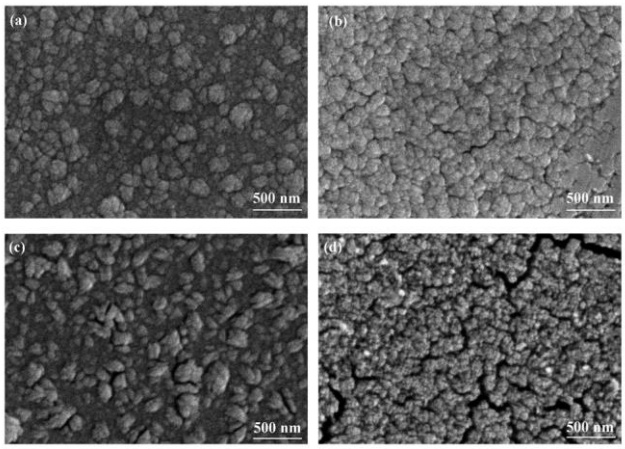

Fig. 3 The SEM images of (a) as-deposited thin films and thin films annealed at (b) 300 ℃, (c) 400 ℃, and (d) 500 ℃.

The optical properties of SnS thin films were measured to get the optical band gaps. Fig. 4 shows the surface reflectance of SnS thin films. The average surface reflectance of as-deposited SnS thin films is 3.52% in the wavelength ranging from 400 nm to 900 nm. For annealed SnS thin films, the average surface reflectance is 2.88%, 4.29%, and 2.85% when the annealing temperatures are 300 °C, 400 °C, and 500 °C, respectively. Fig. 5 shows the transmittances of SnS thin films with and without annealing. For all the SnS thin films, due to the direct band-to-band absorptions, the transmittances reduce with the decreased wavelength.

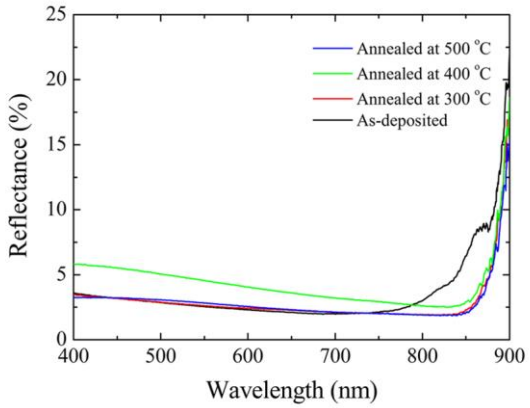

Fig. 4 The reflectance of prepared SnS thin films.

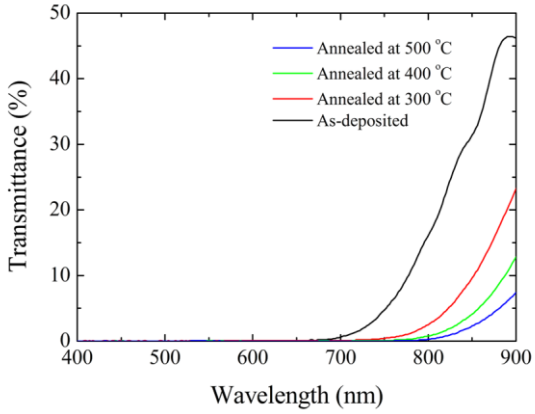

Fig. 5 The transmittances of prepared SnS thin films.

The absorption coefficient α of SnS thin films can be calculated from the equation

$$\alpha = \frac{1}{d}\ln\left(\frac{1-R}{T}\right) \tag{1}$$

where d, R, and T are the thickness, reflectance, and transmittance of SnS thin films, respectively [17].

The direct optical band gaps of SnS thin films can be deduced from the equation

$$(\alpha h\nu)^2 = C\left(h\nu - E_g\right) \tag{2}$$

where $h\nu$ is the photon energy, C is a constant, E_g is the direct optical band gap [10,12]. Fig. 6 shows the $(\alpha h\nu)^2$–$h\nu$ curves of all SnS thin films. In Fig. 6, the absorption coefficients of all SnS thin films are in the 10^4 cm^{-1} orders, which are suitable for thin film solar cell applications. Only a

SnS thickness of about 1 μm is needed to absorb most of incident photons. It can significantly reduce the total thickness of solar cells. In addition, the absorption coefficients of SnS thin films enhance with increasing annealing temperature. In Fig. 6, the linear relations between $(\alpha h\nu)^2$ and $h\nu$ are observed in the high photon energy region. By the extrapolation of linear region of $(\alpha h\nu)^2$–$h\nu$ curves to $h\nu$ axis, the intercept of $h\nu$ axis gives the direct optical band gap. The direct optical band gap of as-deposited SnS thin films is determined to be 1.54 eV. For annealed thin films, the direct optical band gaps are 1.42 eV, 1.41 eV, and 1.38 eV for thin films annealed at 300 °C, 400 °C, and 500 °C, respectively. These direct optical band gaps are close to the reported values [6,10–14]. The enhanced absorptions and decreased direct band gaps are also reported for the evaporated SnS thin films [3,19]. The reduced optical band gaps result from the quantum confinement effect induced by the increasing grain sizes with annealing temperature [3,19].

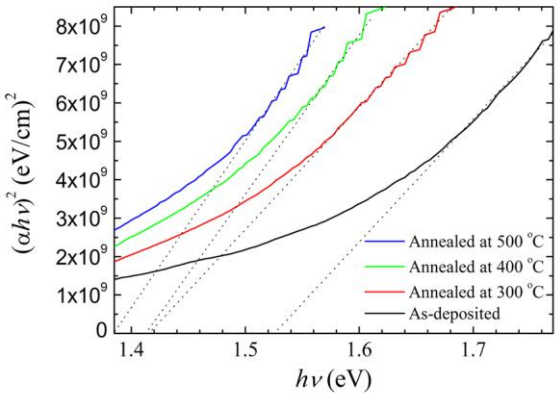

Fig. 6 The $(\alpha h\nu)^2$–$h\nu$ curves of prepared SnS thin films.

4. Conclusions

The semiconducting SnS thin films were fabricated by magnetron sputtering and post vacuum annealing. The influences of annealing temperature on the properties of SnS thin films were studied. The XRD results indicate that the as-deposited and annealed SnS thin films have preferred orientation along the (040) plane. The crystallinity of thin films enhances with increasing annealing temperature. By the observation of SEM images, the cracks and voids in the thin film surface enhance with the increase of annealing temperature. All the SnS thin films show absorption coefficients in the 10^4 cm^{-1} orders. The direct optical band gaps of annealed SnS thin films vary from 1.38 eV to 1.42 eV.

Acknowledgements

This work was supported by China Postdoctoral Science Foundation funded project (No. 2012M521575).

References

[1] M. A. Green, K. Emery, Y. Hishikawa, W. Warta, E. D. Dunlop, Prog. Photovoltaics **22**, 1 (2014).

[2] H. Katagiri, K. Jimbo, W. S. Maw, K. Oishi, M. Yamazaki, H. Araki, A. Takeuchi, Thin Solid Films **517**, 2455 (2009).
[3] O. E. Ogah, K. R. Reddy, G. Zoppi, I. Forbes, R. W. Miles, Thin Solid Films **519**, 7425 (2011).
[4] B. Ghosh, M. Das, R. Banerjee, S. Das, Sol. Energy Mater. Sol. Cells **92**, 1099 (2008).
[5] A. Sanchez-Juarez, A. Tiburcio-Silver, A. Ortiz, Thin Solid Films **480–481**, 452 (2005).
[6] F. Jiang, H. L. Shen, W. Wang, L. Zhang, J. Electrochem. Soc. **159**, H235 (2012).
[7] K. T. R. Reddy, N. K. Reddy, R. W. Miles, Sol. Energy Mater. Sol. Cells **90**, 3041 (2006).
[8] C. C. Huang, Y. J. Lin, C. J. Liu, Y. W. Yang, Microelectron. Eng. **110**, 21 (2013).
[9] K. Hartman, J. L. Johnson, M. I. Bertoni, D. Recht, M. J. Aziz, M. A. Scarpulla, T. Buonassisi, Thin Solid Films **519**, 7421 (2011).
[10] T. Ikuno, R. Suzuki, K. Kitazumi, N. Takahashi, N. Kato, K. Higuchi, Appl. Phys. Lett. **102**, 193901 (2013).
[11] R. W. Miles, O. E. Ogah, G. Zoppi, I. Forbes, Thin Solid Films **517**, 4702 (2009).
[12] K. T. R. Reddy, P. P. Reddy, R. Datta, R. W. Miles, Thin Solid Films **403**, 116 (2002).
[13] F. Jiang, H. L. Shen, C. Gao, B. Liu, L. Lin, Z. Shen, Appl. Surf. Sci. **257**, 4901 (2011).
[14] E. Guneri, C. Ulutas, F. Kirmizigul, G. Altindemir, F. Gode, C. Gumus, Appl. Surf. Sci. **257**, 1189 (2010).
[15] K. Takeuchi, M. Ichimura, E. Arai, Y. Yamazaki, Sol. Energy Mater. Sol. Cells **75**, 427 (2003).
[16] T. Miyawaki, M. Ichimura, Mater. Lett. **61**, 4683 (2007).
[17] R. E. Banai, H. Lee, M. A. Motyka, R. Chandrasekharan, N. J. Podraza, J. R. S. Brownson, M. W. Hom, IEEE J. Photovoltaics **3**, 1084 (2013).
[18] B. Ghosh, R. Bhattacharjee, P. Banerjee, S. Das, Appl. Surf. Sci. **257**, 3670 (2011).
[19] P. Jain, P. Aruna, Thin Solid Films **548**, 241 (2013).